

JGR Space Physics

RESEARCH ARTICLE

10.1029/2022JA030712

Key Points:

- We discuss shifts of Ganymede's footprint in either poleward or equatorward directions
- Use of a magnetodisc model indicates connection between footprint shifts, hot plasma temperature and Iogenic mass loading rate
- Model-observations comparison reveal that solar wind compression of the magnetosphere can produce poleward shift of the footprint

Correspondence to:

T. Promfu and S. Wannawichian,
tatphicha_p@cmu.ac.th;
suwicha.w@cmu.ac.th







Citation:

Promfu, T., Nichols, J. D., Wannawichian, S., Clarke, J. T., Vogt, M. F., & Bonfond, B. (2022). Ganymede's auroral footprint latitude: Comparison with magnetodisc model. *Journal of Geophysical Research: Space Physics*, 127, e2022JA030712. <https://doi.org/10.1029/2022JA030712>

Received 3 JUN 2022

Accepted 5 DEC 2022

Ganymede's Auroral Footprint Latitude: Comparison With Magnetodisc Model

T. Promfu^{1,2} , J. D. Nichols³ , S. Wannawichian^{1,2} , J. T. Clarke⁴ , M. F. Vogt⁴ , and B. Bonfond⁵ 

¹Department of Physics and Materials Science, Faculty of Science, Chiang Mai University, Chiang Mai, Thailand, ²National Astronomical Research Institute of Thailand (Public Organization), Chiang Mai, Thailand, ³Department of Physics and Astronomy, University of Leicester, Leicester, UK, ⁴Center for Space Physics, Boston University, Boston, MA, USA, ⁵LPAP, STAR Institute, Université de Liège, Liège, Belgium

Abstract Variations of Ganymede's auroral footprint locations are presented based on observations by the Hubble Space Telescope in 2007 and 2016. The poleward and equatorward shifts of Ganymede's footprint could be influenced by the mass outflow rate from Io and the solar wind compression, as the internal and external factors respectively. We compare our results with Ganymede's footprint mapping based on the magnetodisc model. The mapped footprint in Jupiter's ionosphere shifts equatorward with increased hot plasma parameter, K_h , which is associated with hot plasma pressure. We analyzed the effect of cold plasma number density (N_c), related to the mass outflow rate and connected to the material produced by Io. The results show that the magnetic footprint is shifted equatorward by 0.37° when the mass outflow rate is increased from $800\text{--}2,000\text{ kg s}^{-1}$. Iogenic plasma has a strong influence on the stretching of the magnetic field lines in Jupiter's middle magnetosphere, causing the equatorward shift of Ganymede's footprint. For external factors, Ganymede's footprint shifted poleward by 0.62° under the influence of solar wind compression while the mass outflow is kept constant at $1,000\text{ kg s}^{-1}$. We present similar locations of Ganymede's footprint based on the field lines mapped as a result of the compensation between an increase of K_h and the solar wind compression. Overall, the location of Ganymede's auroral footprint corresponds with the mass loading rate from Io and the solar wind dynamic pressure.

1. Introduction

The dynamics of Jupiter's magnetosphere are controlled principally by the planet's strong magnetic field, rapid rotation, and Io plasma source, and to a lesser extent the solar wind (Khurana et al., 2004; Krupp et al., 2004). Jupiter's magnetosphere is often divided into three regions, which are the inner magnetosphere ($<10 R_J$) characterized by a mostly-dipolar magnetic field configuration, the middle magnetosphere (~ 10 to $40 R_J$), in which the field lines are radially distended into a magnetodisc configuration, and the outer magnetosphere ($>40 R_J$) characterized by disordered but predominantly southward field, and the magnetotail (Khurana et al., 2004). The processes occurring within Jupiter's magnetosphere can be diagnosed by observations of the planet's auroral emissions. Jupiter's far-ultraviolet (FUV) auroras are Lyman alpha and Lyman and Werner H_2 band emission resulting from particle precipitation (Clarke et al., 2004). The FUV morphology of the auroras, with primary components being the main emission, outer emission, satellite footprints, and polar emission is shown in Figure 1. The main emission is mapped to the middle region of the magnetosphere (average radial distance ~ 35 to $40 R_J$ (Vogt et al., 2015)) and is thought to be associated with magnetosphere-ionosphere (M-I) coupling currents (Cowley & Bunce, 2001; Nichols et al., 2020). Io is a significant source of plasma mass in the Jovian magnetosphere, with volcanoes on Io releasing sulfur dioxide at a canonical rate of $1,000\text{ kg s}^{-1}$ (Kivelson et al., 2004), a substantial fraction of which is ionized to form sulfur and oxygen plasma. In addition, Bagenal and Delamere (2011) presented the charge densities from the Voyager Plasma Science instrument as a result of the current measured in the range of $10\text{--}6,000\text{ eV}$. Additionally, the materials from Io appear to be supplied constantly which could be associated with the M-I interaction. The plasma number density variation is connected to the mass outflow rate, mainly related to Io volcanic materials. Moreover, the mass loading from Io could also be a result of the sublimation of material from the surface of Io and the plasma-atmosphere interaction, which can be affected by the change in the electron temperature and plasma density (Bolton et al., 1997; Roth et al., 2020; Saur et al., 1999).

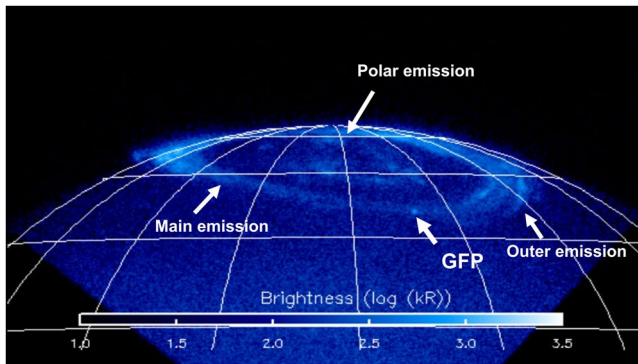


Figure 1. Jupiter's aurora from HST observation on 3 June 2016. The arrows indicate features of Jupiter aurora which are main emission, polar emission, outer emission and Ganymede's auroral footprint (GFP).

The interaction of the rapidly rotating field and plasma with the slower satellites and newly-ionized plasma is complex and leads to a number of distinct features of the satellite auroral footprints. These features are described in detail in Bonfond et al. (2008) and are apparent in each satellite footprint though with different morphology and details of the local interaction. Briefly, as the magnetospheric field and plasma convect past a satellite, the flow is diverted around the moon and the field is distorted, creating a structure called an Alfvén wing (Drell et al., 1965). Alfvén waves propagate along these wings and they can accelerate particles (Lysak & Song, 2003), which then precipitate into the ionosphere and cause an auroral feature known as the Main Alfvén Wing (MAW) spot. The Alfvén waves are partially reflected in the density gradients at the boundaries of the region of dense equatorial plasma or at the Jovian ionosphere leading to Reflected Alfvén wing spots (Bonfond et al., 2017; Hess et al., 2010; Schlegel & Saur, 2022). In addition, beams of electrons propagate along field lines leading to Transhemispheric Electron Beam (TEB) spots (Bonfond et al., 2008). Juno observations have confirmed the Alfvénic wave power associated with the satellite footprints (Gershman et al., 2019; Moirano, Gomaz Casajus et al., 2021; Moirano, Mura et al., 2021; Sulaiman et al., 2020; Szalay et al., 2020). Szalay et al. (2020) presented the peak energy of the precipitating electron along the Alfvén wave to be ~ 11 mW/m² using Juno Jovian Auroral Distributions Experiment (JADE) observation.

This work focuses on Ganymede's auroral footprint. The first detection of Ganymede's footprint spot was presented by Clarke et al. (2002) using the Space Telescope Imaging Spectrograph (STIS) with the Multi-Anode Microchannel Array (25MAMA) detector (bandpass from 1,150 \AA to 1740 \AA) onboard the Hubble Space Telescope (HST). In addition, Bonfond, Hess, Bagenal, et al. (2013) and Bonfond, Hess, Gérard, et al. (2013) presented the UV aurora images taken by HST on 24 May 2007, showing two spots of Ganymede's footprint. The same spots were also observed in the infrared by the Jovian Infrared Auroral Mapper onboard Juno (Adriani et al., 2017; Mura et al., 2018). These two spots correspond to MAW and TEB spots, whose distance of separation is associated with the location of Ganymede in the plasma sheet. The interaction between Jupiter's magnetic field and the satellite is modified by the existence of Ganymede's intrinsic magnetic field (Kivelson et al., 1997), which then acts as the effective obstacle, rather than the moon itself (Jia et al., 2008; Paty et al., 2008; Plainaki et al., 2015, 2016; Saur et al., 2013; Szalay et al., 2020). The interaction is mediated by reconnection between the magnetic fields of Jupiter and Ganymede, and the interaction region is enlarged to encompass a region 8–20 R_G wide in Ganymede's orbital plane (Grodent et al., 2009) (where R_G is the satellite's radius equal to $R_G = 2,634$ km). However, the Ganymede auroral footprint is likely to be driven by broadly similar Alfvénic interaction as described above (Szalay et al., 2020). The orbital radius of Ganymede is $\sim 15 R_J$, that is, in the inner part of the middle magnetosphere where the field is moderately radially stretched from the planetary dipole by currents related to outward forces associated with magnetospheric plasma (Connerney et al., 1981, 2020; Nichols, 2011; Nichols et al., 2015). The magnetic mapping between the satellite's location in the equatorial plane and the auroral footprint in the ionosphere is thus modified from that expected from the planetary field alone, with a fixed equatorial radial distance mapping further equatorward for a more extended field. Such variation in the degree of stretching of the field possibly explains the observed changes in the latitude of the footprint (Grodent et al., 2008). The radial stretching of the field into a magnetodisc configuration is associated with an azimuthal current, whose inward $\mathbf{j} \times \mathbf{B}$ force balances outward forces, which are the plasma pressure gradient, pressure anisotropy, and the centrifugal force of the rotating plasma. For the pressure anisotropy, Nichols et al. (2015) showed that the increase of hot plasma pressure anisotropy ($P_{\parallel e}/P_{\perp e}$) causes the increase of azimuthal current density in the middle magnetosphere, considered to be an additional force resulting in the stretching of the field lines in the magnetodisc model. Force balance models of the magnetodisc consider two plasma populations, that is, a “cold” (few 100 eV) thermal populations of iogenic plasma providing most of the mass but little plasma pressure (Bagenal et al., 2017; Bodisch et al., 2017; Dougherty et al., 2017; McNutt et al., 1981), and a “hot” (20–40 keV) population providing most of the pressure but little mass (Krimigis et al., 1981). The plasma centrifugal force is determined by its radial angular velocity profile, which is governed in the steady state by the parameters of the M-I coupling current system that transfers momentum between the planet and the magnetospheric plasma. Nichols (2011) showed that variations in the ionospheric Pedersen conductance and iogenic plasma mass outflow rate could potentially affect the latitude of the Ganymede footprint, but unrealistically large changes were needed to explain the observed

Table 1
The Summary of the Data Set in This Study

Year	Instrument	DOY	Date
2007	ACS	052–054	21–23 February
		058–059	27–28 February
		061	2 March
		066	7 March
		068	9 March
		131	11 May
		132	12 May
		133	13 May
		137	17 May
		138	18 May
		151	31 May
		154	3 June
		161	10 June
2016	STIS	139–140	18–19 May
		147–148	26–27 May
		155–156	3–4 June
		177–178	25–26 June
		199	17 July

shifts. The hot plasma pressure gradient is generally the largest contribution to the radial force balance, particularly in the inner region, and Nichols et al. (2015) thus went on to show that variations in the hot plasma pressure over the modeled range (Caudal, 1986), based on the observed value of hot plasma temperature by Krimigis et al. (1981), would be sufficient to explain the footprint shifts observed by Grodent et al. (2008) and Bonfond et al. (2012). The spacing between the multiple spots of the Ganymede auroral footprint was found to vary even for the same SIII longitude of Ganymede (Bonfond, Hess, Bagenal, et al., 2013; Bonfond, Hess, Gérard, et al., 2013), apparently in response to the changes in the plasma sheet density. The observations of Ganymede footprint locations by Grodent et al. (2008), Bonfond, Hess, Bagenal, et al. (2013), and Bonfond, Hess, Gérard, et al. (2013) considered two footprint observations showing an extreme latitudinal shift, and the modeling work (Nichols et al., 2015) was not referenced to other contemporaneous indications of the state of the system. In this study, we examine a series of HST observations obtained in 2007 and 2016, as shown in Table 1, and consider the effects which might give rise to the shifts in the latitude of the Ganymede footprint observed during these periods in the context of estimated solar wind conditions (external factor) and observations of the Io plasma torus (internal factor).

We compare our results with estimations and observations of the solar wind and Io activity during the observation intervals, in order to examine the effects of internal versus external factors on the location shifts of Ganymede's footprint. Evidence of persistently strong volcanic eruptions on Io from February to the beginning of June 2007 were presented by Spencer et al. (2007), Yoneda et al. (2009), Bonfond et al. (2012), and Yoneda et al. (2013). Spencer

et al. (2007) revealed the continuous thermal emission from the Tvashtar plume from 18 January to 27 May 2007. In addition, Bonfond et al. (2012) using auroral images of Jupiter's northern hemisphere from HST showed the expansion of the main emission on 31 May 2007 (equivalent to Day Of Year 151 or DOY 151) including the location of Ganymede's footprint which shifted ~500 km in equatorward direction. Bonfond et al. (2012) found that the size of the main emission continued to increase from February 2007 to June 2007 and they concluded that this was caused by a consistently strong level of volcanic activities on Io during the HST observations. They also noted an increased number of intense auroral injection signatures, indicative of frequent and strong reconfigurations of the magnetosphere loaded with iogenic plasma. Moreover, Yoneda et al. (2013) using the data from Haleakala Observatory in Hawaii, which was observed from 19 May to 21 June 2007, presented the enhancement of Jupiter's sodium nebula from late May to the beginning of June 2007. Yoneda et al. (2009, 2013) suggested that the increase of Jupiter's sodium nebula brightness corresponds with the rising mass outflow rate from Io. Furthermore, Tsuchiya et al. (2019) measured the density and temperature of the Io plasma torus over 2013–2016 using Hisaki data and presented no evidence of any strong volcanic eruptions during the interval of interest here. It must be noted that, while Tsuchiya et al. (2019) found the decrease of System IV rotation period of the Io plasma torus during the volcanic activities on Io, such activity seemed to affect the electron temperature rather than the total ion mass, corresponding to higher K_p . Tsuchiya et al. (2018) also suggested that the plasma torus radial distribution from 6 to 8 R_J takes ~15 days from the beginning of eruption (Yoneda et al., 2015). As a result, the connection between the volcanic eruptions on Io and the variations in the plasma environment in Jupiter's magnetosphere is highly complex (Moirano, Gomaz Casajus et al., 2021; Moirano, Mura et al., 2021; Roth et al., 2020). In addition, Kita et al. (2019) presented the increasing solar wind dynamic pressure during the interplanetary coronal mass ejection and corotating interaction region (CIR) events which were detected by JADE instrument (McComas, Alexander et al., 2017; McComas, Szalay et al., 2017). Interplanetary coronal mass ejection was reported during DOY 140–145 and CIR was reported during DOY 150–155 (CIR), and DOY 170–176 (McComas, Alexander et al., 2017; McComas, Szalay et al., 2017). In addition, the effect of solar wind compression was presented by Nichols et al. (2009). They presented two data sets for the mean deviations of the main emission from the reference position observed in 2007, during February–March (DOY 051–070) and May–June (DOY 131–162). The results show that the main emission located poleward at approximately 0.5° – 1° from the reference position during the solar wind compression. Nichols et al. (2009) also found that the main

emission located approximately 2° equatorward on DOY 151 which is consistent with strong volcanic activities on Io (Yoneda et al., 2013). The volcanic activity on Io affects the low latitude emission in the equatorward direction from the main emission during ~ 10 days after sodium nebula enhancement (Nichols et al., 2017). Nichols et al. (2017) using the interplanetary data (McComas, Alexander et al., 2017; McComas, Szalay et al., 2017) showed that the UV auroral power and the magnitude of the interplanetary magnetic field increased during solar wind compression, but decreased during the rarefaction. Overall, we find the principal effects to be the mass outflow which supplies from volcanic activity on Io can cause the expansion of the main emission location, and could possibly affect the location of the Ganymede footprint as well. Furthermore, we assess the impact of the solar wind dynamic pressure coupled with the plasma from Io to study the behavior of the shifts in Ganymede's footprint location corresponding with various solar wind dynamic pressures, which is shown in the Discussion section.

2. Observations and Data Analysis

We consider Jupiter FUV images obtained by two instruments onboard HST, which are the STIS and Advanced Camera for Surveys (ACS). We employ data obtained in 2007 using Solar Blind Camera (SBC) on the ACS, with the F115LP (1,150–1,700 Å) and F125LP (1,250–1,700 Å) filters and exposure times between 30 and 100s. The wavelength bandpass of ACS/SBC is 1,150–1,700 Å, which includes H Ly- α line, H₂ Lyman bands and Werner bands (Clarke et al., 2009; Wannawichian et al., 2010). We also use data obtained in 2016 using the HST/STIS Multi-Anode Microchannel Array detector with the F25SRF2 (1,300–1,740 Å) filter (Nichols et al., 2017). For this work, FUV time tag data were extracted using 100s integration time. For the ACS data, the locations of Ganymede's auroral footprint were separated into two groups which are February - March (DOYs 052–054 and 058–059 in February, 061, 066, 068, and 081 in March) and May - June (DOYs 131–133, 137–138, and 151 in May, 154, and 161 in June). For the STIS data, the locations of Ganymede's auroral footprint were compared between May (DOYs 139–140, 147–148), June (DOYs 155–156, 177–178), and July (DOY 199). The summary of our data set is shown in Table 1.

The images were processed using the Boston University reduction pipeline (Clarke et al., 2009), which includes dark image subtraction, flat-field correction, and instrumental geometric distortion correction. The brightness was converted from counts to kilo-Rayleighs ($1 \text{ kR} = 10^9 \text{ photons cm}^{-2} \text{ s}^{-1}$) using the conversion factor from Gustin et al. (2012) for a color ratio of 1.04, under the assumption of no methane absorption for Ganymede footprint emission. The color ratio is the ratio of auroral emission in two wavelength bands, one subject to strong hydrocarbon absorption and the other no hydrocarbon absorption. The images of Jupiter auroral region, as shown in Figure 1, were projected onto a latitude and longitude grid about 240 km above 1 bar level at Jupiter's ionosphere. For the analysis of Ganymede footprint's position, the footprint is considered to be 900 km above the 1 bar level (Bonfond, 2010; Tao et al., 2011). For the location of Ganymede's footprint, we identify the brightness centroid position of Ganymede's footprint in Jupiter's ionosphere, as shown in Figure 2. The background brightness, which is the intensity of the adjacent area, approximately 1° – 2° from the footprint position, was subtracted from the integrated brightness of footprint emission in the image, giving, as a result, the Ganymede's footprint brightness as for the previous study by Wannawichian et al. (2010). The position uncertainty is considered to be a result of three causes. First, since the centroid is fitted with Gaussian distribution, the standard error was determined based on the FWHM of the average intensity profile in close proximity to the footprint centroid, as shown in Figure 2. The second cause of the uncertainty is due to the finding of the planet center. The North-South fitting during the finding of the planet center is approximately 1–2 pixels uncertainty (corresponding to 0.1 – 0.2°), while the East-West fitting is approximately 1–3 pixels (corresponding to 0.1 – 0.3°). However, the East-West uncertainty is limited due to the lack of a clearly defined terminator on one side of the planet (Clarke et al., 2009). Lastly, the altitude uncertainty of the brightness peak uncertainty is assumed to be ~ 100 km (Bonfond, 2010), which adds uncertainty to the positioning of approximately 0.025° . Since the images were taken with two different instruments (STIS and ACS), test cases have been run to ensure that there is no systematic offset in the latitude of the footprints between the different cameras. Comparisons of the latitudes of locus of Io footprints have shown that the instruments do not show any systematic offset within 0.2° . Accordingly, the determination of footprint position can be reasonably precise. In addition, to avoid any possible systematic effect, we chose the case study between the observations with the same instruments. For the method of removing reflected sunlight, we create a simulated disk of reflected sunlight, convolve it with the point spread function, and subtract the simulated disk from the original images (Clarke et al., 2009). Overall, we have determined the location of the footprint in 436

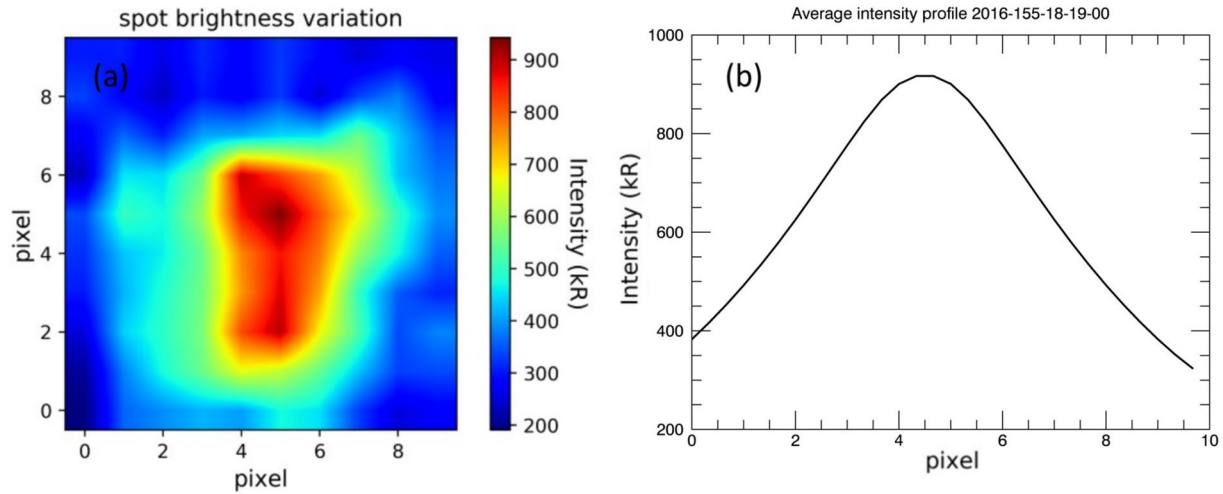


Figure 2. Intensity distribution around the location of Ganymede's auroral footprint was taken on 3 June 2016 (a). The average intensity profile of the emission near the centroid location is indicated by the black solid line (b). The FWHM of the intensity distribution is employed to consider the uncertainty of the footprint location. It should be noted that this is the simplification in comparison to the real shape of the footprint, corresponding to the angular size of 0.025 arcsec per pixel (Clarke et al., 2009), whose length, width, and height might be different from each other.

individual images, providing the primary data set employed in this paper. From our overall results, Ganymede footprint location were found to shift either poleward or equatorward direction. We expect that the shift in Ganymede footprint location could be affected by both internal and external factors. Thus, we employ the magnetodisc model to interpret the effects of these two factors which will be discussed in the next section.

3. Magnetodisc Model

In this work, the magnetodisc model of Nichols et al. (2015) was used to estimate the influence on the magnetodisc of the solar wind compressions and variation in Io volcanic activity. This is done principally by varying the magnetopause radius, hot plasma parameter (K_h), iogenic mass outflow rate, and cold plasma number density in this model as discussed below. The K_h parameter is related to the hot plasma pressure associated with the hot plasma outside Io torus (Caudal, 1986; Nichols et al., 2015), especially the perpendicular pressure at the equatorial distance of more than $7.5 R_J$. It is, however, important to note that this is a quasi-steady state model, which enables consideration of the effects on the mapping from the equator to the ionosphere over timescales longer than the few hours following for example, impulsive solar wind compressions, the transient effects of which are thus not described by the present formulation. Nevertheless, Nichols (2011); Nichols et al. (2015) indicated that variation of the values of the iogenic plasma mass outflow rate and the hot plasma parameter can affect the ionospheric mapping of Ganymede, with the latter being most influential, within typically observed ranges. They reported that for different K_h , between $1-2.5 \times 10^7 \text{ Pa m T}^{-1}$, the mapping locations of Ganymede's footprint in colatitude vary between 16.6° and 17.6° , respectively. Thus, the variation of the K_h could be a significant influence on the location shift of Ganymede's footprint in the ionosphere.

The details of the model have been discussed elsewhere Nichols (2011) and Nichols et al. (2015, 2020), such that here we provide a brief introduction. The model computes iteratively the vector potential $\mathbf{A}(\rho, z) = A(\rho, z)\hat{\phi}$ from an azimuthal current $\mathbf{j}(\rho, z) = j(\rho, z)\hat{\phi}$ using Ampère's law, $\nabla^2 \mathbf{A} = -\mu_0 \mathbf{j}$. Mapping between the equator and ionosphere is achieved using the flux function (F), which is constant along a given field line and is related to the vector potential via $F = \rho A$, where ρ is the cylindrical radius. Thus, the magnetic mapping between the equatorial plane and ionosphere was obtained via the equality of $F_e = F_i$, where F_e and F_i are the equal flux function values for magnetically conjugate points in the equatorial magnetodisc and ionosphere, respectively. Assuming a dipolar ionospheric field, the flux function in the ionosphere is given by

$$F_i = B_J \rho_i^2 = B_J R_J^2 \sin^2 \theta_i \tag{1}$$

where θ_i is the magnetic co-latitude, B_j is the equatorial magnetic field strength, ρ_i is the perpendicular distance from the magnetic axis, and R_j is the equatorial radius of Jupiter ($\sim 71,492$ km). The momentum equation for a rotating plasma is given by

$$\rho_m \frac{d\mathbf{v}}{dt} = \mathbf{j} \times \mathbf{B} - \text{div } \mathbf{P} \quad (2)$$

where ρ_m is plasma mass density, \mathbf{v} is the plasma bulk velocity, \mathbf{P} is the pressure tensor, and \mathbf{B} is Jupiter's poloidal magnetic field. Considering gyrotropic pressure and rearranging for the perpendicular current \mathbf{j}_\perp , we have

$$\mathbf{j}_\perp = \frac{\hat{\mathbf{b}}}{B} \times \left[\rho_m \frac{d\mathbf{v}}{dt} + \nabla p_\perp + (p_\parallel - p_\perp) (\hat{\mathbf{b}} \cdot \nabla) \hat{\mathbf{b}} \right] \quad (3)$$

where $\hat{\mathbf{b}} = (b_\rho, b_z)$ is the unit vector along the poloidal magnetic field. The terms on the right-hand side represent the centrifugal force, pressure gradient, and pressure anisotropy forces, which are dependent on plasma and M-I coupling parameters, for example, mass outflow rate (\dot{M}), hot plasma parameter (K_h) and cold plasma number density (N'_c). The model is initiated using a dipole magnetic field and proceeds by iteration until convergence, as described by Nichols (2011) and Nichols et al. (2015). The model considers two plasma populations, a "cold" centrifugally-confined population of ~ 100 eV (Bagenal & Delamere, 2011; Bagenal et al., 2017; Bodisch et al., 2017; Dougherty et al., 2017; Frank & Paterson, 2002; McNutt et al., 1981) dominating the centrifugal force, and a "hot" population corresponding to the ~ 20 – 40 keV observed by Krimigis et al. (1981) providing most of the plasma pressure. The former is characterized in the model by a given flux tube content and angular velocities computed using 'Hill-Pontius' theory (Hill, 1979; Pontius, 1997) which considers the steady outflow of azimuthal angular velocity plasma (ω) associating with the flux function (F_c) and the north-south magnetic field threading on the equatorial plane ($|B_{ze}|$) (Nichols et al., 2015). A key parameter in determining the plasma angular velocity is the plasma mass outflow rate (\dot{M}). The plasma pressure of the hot particle population is characterized by the K_h parameter, given by

$$K_h = P_{hLe}(F) V_h(F) \quad (4)$$

where $V_h(F)$ is the flux tube volume. The K_h parameter varies between 1 – 5×10^7 Pa m T $^{-1}$, based on the observation of the hot plasma outside Io torus from Pioneer, Voyager 1 and 2 spacecraft (Caudal, 1986).

In this study, the simulation was used to investigate the effect of enhanced Io activity on the magnetic mapping by varying the mass outflow rate (\dot{M}) from 800 to 2,000 kg s $^{-1}$, where the cold plasma number density (N'_c) is proportional to \dot{M} (Nichols, 2011) as described by

$$N'_c = \left(\frac{\dot{M}}{1000} \right) N_c \quad (5)$$

$\dot{M} = 1,000$ kg s $^{-1}$ was set as a reference and $N_c = 8.1 \times 10^{21}$ ions/Wb (Frank & Paterson, 2002; Nichols, 2011). Additionally, the enhanced mass outflow rate from Io causes the increase of the plasma density which is transported outward from Io's vicinity toward the middle magnetosphere and affects the equatorial pressure in the magnetosphere and could have a correlation with the enhancement of plasma heating in Jupiter's magnetosphere, which will be discussed in detail in the Discussion section. The connections between \dot{M} and K_h were proposed by Tsuchiya et al. (2019). Tsuchiya et al. (2019), using a dual hot electron model based on Steffl et al. (2008), presented the increases of the azimuthal amplitudes of torus composition. They concluded that the rotation period of Io plasma torus decreased coincident with an increase in Io's volcanic activity. Moreover, the decrease in the rotation period of Io plasma torus occurred when the electron temperature in the plasma torus increases. Thus, K_h could be increased due to higher electron temperature as well, because the electron temperature in the plasma torus can be raised by the Coulomb interactions between electrons in the plasma torus and the hot electrons. Thus, in our simulation, we test the variation of the outcomes, due to the increase of the hot plasma parameter (K_h) from 1.25 – 4.5×10^7 Pa m T $^{-1}$. We considered the effects of the parameters above which are \dot{M} , K_h , where N'_c is a function of \dot{M} , along with the solar wind compression by reducing the size of the magnetosphere from 80 to 50 R_j , where the enhancement of K_h could be associated with the magnetosphere shrinkage due to the adiabatic compression. It must be noted that the hot plasma temperature in this work is considered based on the analysis of Krimigis et al. (1981), previously used in the magnetodisc model by Nichols et al. (2015). Recently, Dougherty

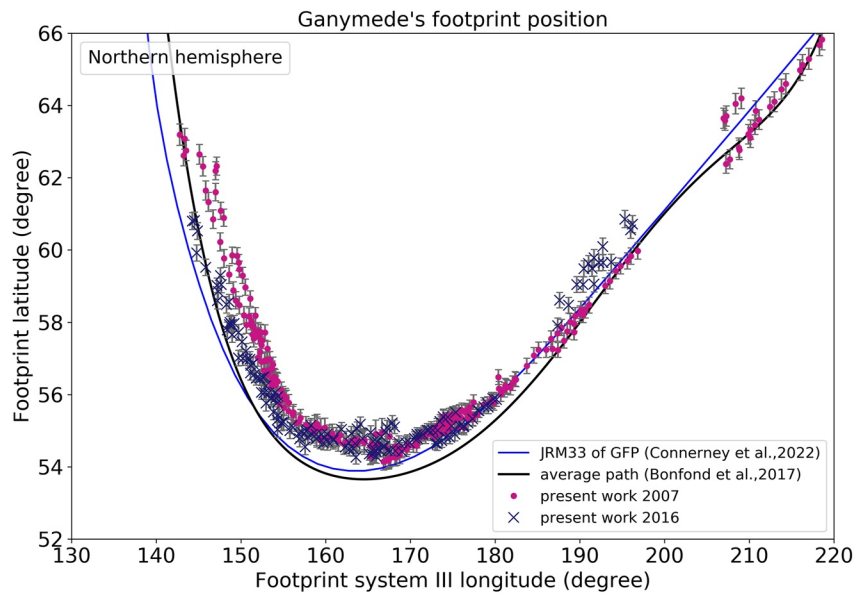


Figure 3. The locations of Ganymede's auroral footprint in the northern hemisphere, during two HST campaigns in 2007 (pink circles) and in 2016 (blue crosses), in comparison with the average path from Bonfond et al. (2017) (black line) and the mapped Ganymede's footprint location from JRM33 Connerney et al. (2022) (blue line).

et al. (2017) found that the hot plasma temperature could reach at most ~ 1 keV at Ganymede orbit. For the current analysis, the model results were qualitatively compared with the Ganymede footprint observation to study the effect of location shifts in either equatorward or poleward direction. Therefore, the quantitative study of hot plasma temperature's effect on the model result will be proceeded in future analysis.

4. Results

4.1. Ganymede Footprint Location

The Ganymede footprint locations for all data listed in Table 1 are presented in Figure 3, in which the variation of the position can be seen and focused on specific events, as shown in Figure 4. In Figure 3, we have compared our Ganymede footprint locations in the northern hemisphere with the average path determined by Bonfond et al. (2017) (black line). Moreover, our Ganymede footprint locations are compared with the mapped Ganymede footprint contour presented by Connerney et al. (2022) using the Juno reference model through perijove 33 (JRM33) internal field model (blue line), and the Connerney et al. (2020) magnetodisc model. We note that the average Ganymede footprint path is not circular, due to the non-dipolar nature of the planet's internal field (Connerney et al., 2018, 2020), with a relatively sharp poleward “kink” in the region $\sim 140^{\circ}$ – 150° System III (SIII) longitude. In the kink region, the Ganymede footprint's locations from both Bonfond et al. (2017)'s average path and our data are constantly shifted in a poleward direction, in comparison with the mapped path by JRM33. This poleward shift could be associated with the local time effect, in which, based on the magnetodisc model, the magnetic field lines are less stretched on the dusk side corresponding to the poleward shift of the footprint (Khurana & Schwarzl, 2005). Moreover, HST had been observing the footprint on the dusk side more often than on the dawn side. As a result, Ganymede's footprint locations were found to shift to higher latitudes.

The distance shifts of Ganymede's footprint from the mapped footprint contour (Connerney et al., 2022) corresponding to Figure 3 in 2007 and 2016 are shown in Figure 4, separately for February–March 2007 (a), May–June 2007 (b), and May–July 2016 (c). We consider four pairs of specific cases of Ganymede's footprint locations at similar System III longitude and Central Meridian Longitude (CML), represented by four gray areas in Figure 4. These criteria constrain the positions of Ganymede to be similar in Jupiter's magnetosphere configuration. In 2007, Ganymede's footprint mostly located in poleward directions from the mapped footprint location with shifted angles of approximately 0.5° – 3° (above the black line) at longitude $\sim 145^{\circ}$ – 160° and located near the mapped footprint location at system III longitude $\sim 170^{\circ}$ – 200° (Figures 4a and 4b). Ganymede's footprint locations in

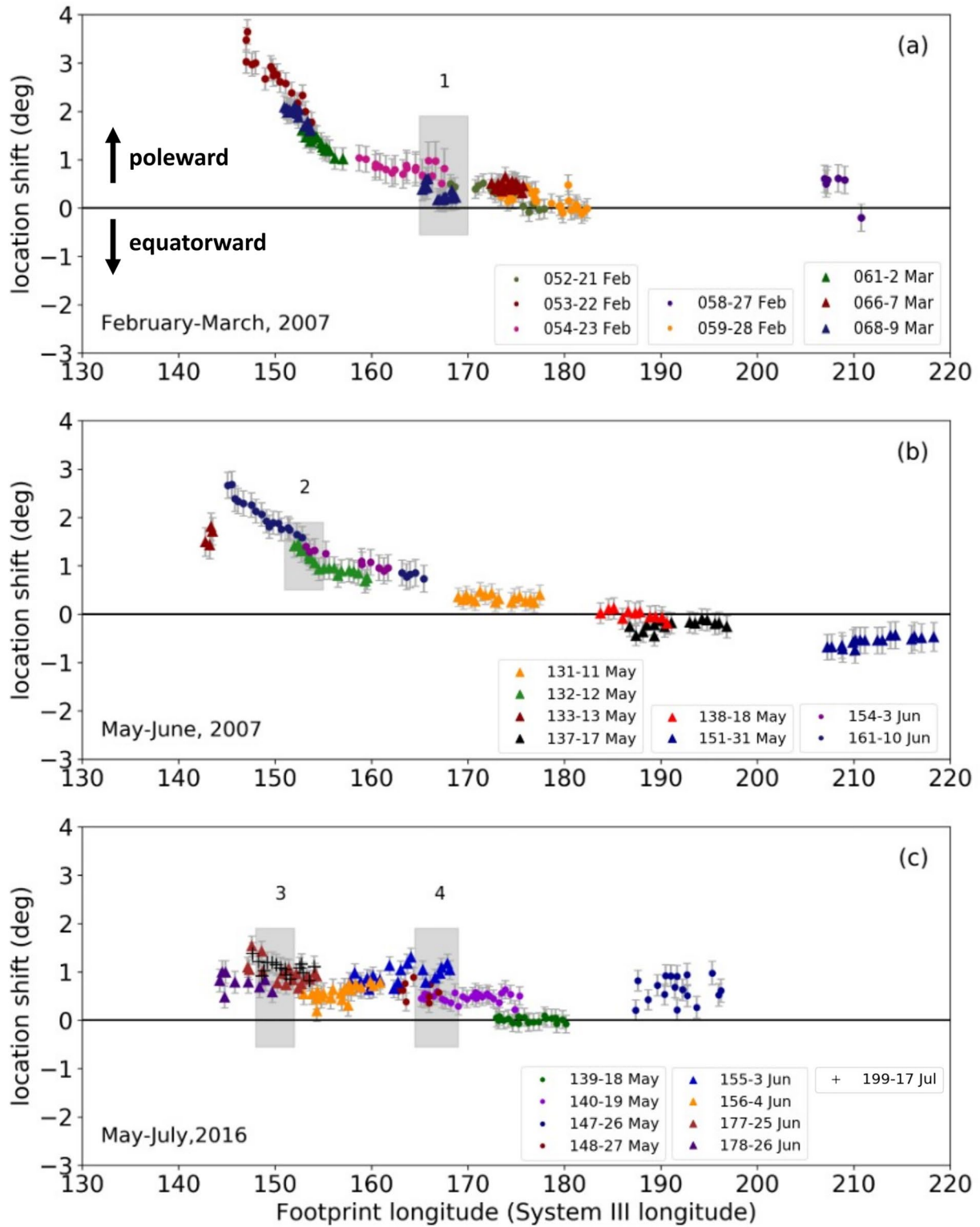


Figure 4. The shifts of Ganymede's auroral footprint location in the northern hemisphere, from mapped Ganymede's footprint location from JRM33 (black solid line) (Connerney et al., 2022), are presented based on the HST observations during February and March 2007 (a), May and June 2007 (b), and from May to July 2016 (c). The footprint location shifts are mainly focused for 4 cases, as labeled with numbers in each panel. All the images in the focused events are constrained to have similar CMLs.

2007 on DOY 151 (Figure 4b) shifted equatorward in comparison to Ganymede's footprint locations observed on DOY 058 (Figure 4a). This could correspond to the higher brightness of sodium nebula which is observed in late May (Yoneda et al., 2009), considered as an indicator of increased Iogenic plasma mass which is discussed as an internal factor in this work. Moreover, Bonfond et al. (2012) presented the expansion of the main emission in late May 2007 which might connect to the increased volcanic activity on Io. Thus, while the volcanic materials from Io are contributed to the plasma sheet, the density increase could affect the stretching of the magnetic field line corresponding to the increase of azimuthal current density, which is enhanced along the equatorial plane. These results were presented by Nichols et al. (2015) and shown in our detailed analysis in the next section.

For all specific cases, Case 1 (Figure 4a), in 2007, Ganymede's footprint locations observed on DOY 054 shifted poleward in comparison to Ganymede's footprint location observed on DOY 068. For Case 2 (Figure 4b), Ganymede's footprint was detected at similar locations during three events in 2007 on DOY 132, DOY 154, and DOY 161. For Cases 3 and 4 (Figure 4c), Ganymede's footprint was observed in 2016. For Case 3, Ganymede's footprint locations observed on DOY 199 shifted poleward in comparison to Ganymede's footprint locations observed on DOY 178. For Case 4, Ganymede's footprint locations observed on DOY 148 slightly shifted equatorward in comparison to the footprint locations observed on DOY 155.

4.2. Magnetodisc Model Results

The results based on the magnetodisc model in Figure 5 show the effects of the K_h , the mass outflow rate (\dot{M}), which is related to the cold plasma number density (N_c') in the magnetosphere and angular velocity of Io plasma torus, and the solar wind compression on the field line mapping from a radial distance in the equatorial plane to colatitude position of magnetic footprint in the ionosphere. The modeled results show that the location of the field line mapping from Ganymede position ($\sim 15 R_J$ from Jupiter) tends to move the magnetic footprint equatorward if the K_h increases as shown in Figure 5a. The mapping of the field lines can be calculated by considering the flux function between the mapped positions, on the equatorial plane and ionosphere, under the assumption of an axisymmetry dipole field (Equation 1).

In addition, the influence of solar wind compressions and plasma variability which could be influenced by mass outflow rate \dot{M} , upon field line mapping near Ganymede was considered. Figure 5a shows the variation of magnetic field line mapping considering the condition of the K_h and the size of Jupiter's magnetopause, which can be varied as a means of simulating the solar wind compression. The increasing of the K_h results in the mapped magnetic footprint in the ionosphere shifting in an equatorward direction for the magnetopause boundary at about $80 R_J$ (solid lines) corresponding to Nichols et al. (2015) which show the effects of the K_h on the azimuthal current density. Nichols et al. (2015) demonstrated that the four contributions to the azimuthal current density are restricted on the equatorial plane with the increase of the K_h . As a result, the magnetic field line can be stretched out to a larger radial distance. Thus, the structure of the field line changes with the variation of current density distribution in the magnetosphere. In the case of solar wind compression, causing the magnetopause boundary to be nearer to the planet, for example, at $50 R_J$ (dash line), the mapped magnetic field lines shift in a poleward direction, for the same K_h . In particular, from Ganymede's orbit at $15 R_J$, the mapped position of the Ganymede ionospheric footprint for the case of the solar wind compression could be comparable to the case of increasing K_h , for example, considering the blue solid line ($K_h = 2.5 \times 10^7 \text{ Pa m T}^{-1}$ and magnetopause distance at $80 R_J$) in comparison with yellow dash line ($K_h = 3.5 \times 10^7 \text{ Pa m T}^{-1}$ and magnetopause distance at $50 R_J$), shown in Figure 5a. Thus, it is possible that solar wind compression could cause the increases of the K_h in Jupiter's magnetosphere resulting in similar mapped locations of the magnetic footprint in Jupiter's ionosphere. Even though in this work, the model assumes that the K_h and the magnetosphere size are independent, there is actually the feedback between the magnetospheric shrinkage and its heating. Therefore, a self-consistent model, which can explicitly determine the relationship between the hot plasma pressure and the variation in magnetosphere size, should be conducted for future work. Figure 5b shows the effect of the variation of mass outflow rate (\dot{M}), corresponding to the cold plasma number density. The result shows that the mapped magnetic field footprint shifts equatorward as Iogenic mass loading rate increases. At a fixed mass loading rate, under the solar wind compression (dashed lines in Figure 5b), the mapped field lines shift in a poleward direction. The comparison between the Ganymede footprint location and the results from the magnetodisc model will be discussed in the next section.

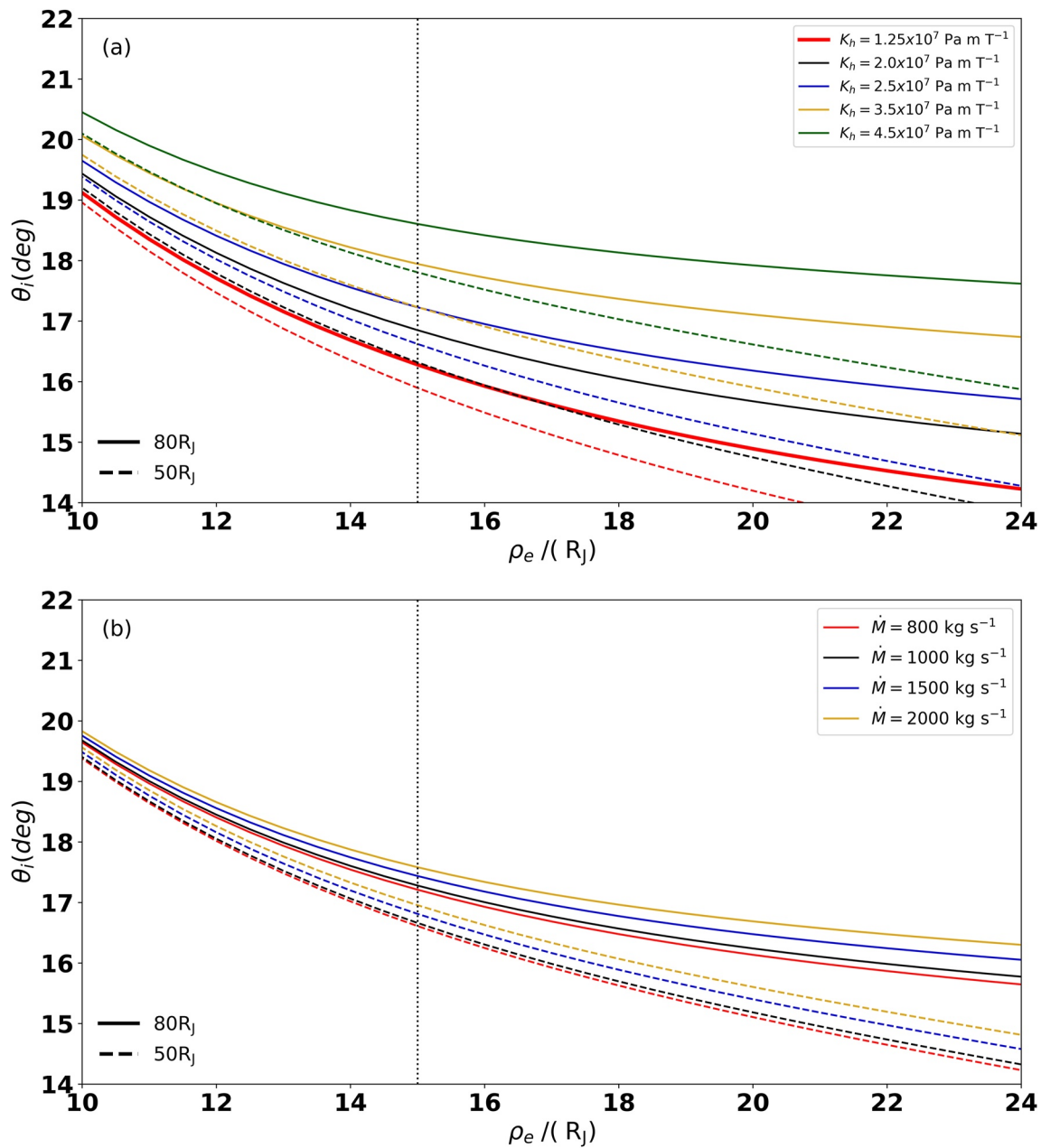


Figure 5. The mapping of the magnetic field lines from the positions on the equatorial plane described by radial distance (ρ_e) to Jupiter's ionosphere in colatitude (θ_i). The mapping is investigated under several conditions; (a) the hot plasma parameter (K_h) varying from $1.25\text{--}4.5 \times 10^7 \text{ Pa m T}^{-1}$, while the mass outflow rate (\dot{M}) is constant ($\dot{M} = 1,000 \text{ kg s}^{-1}$), and (b) the variation of the mass outflow rate (\dot{M}) related to cold plasma number density (N_c) given by Equation 5 while considering $K_h = 2.5 \times 10^7 \text{ Pa m T}^{-1}$, based on magnetodisc model (Nichols et al., 2015). The solid and dash lines represent different sizes of Jupiter's magnetopause, $80 R_J$ and $50 R_J$.

5. Discussion

For the model-observation comparison, we specifically compare the shifts with those expected due to changes in the solar wind dynamic pressure and the iogenic mass outflow rate, as estimated using the Nichols et al. (2015) magnetodisc model. We find that the location shifts of Ganymede's footprint were associated with both solar wind dynamic pressure (external factor) and iogenic mass outflow rate (internal factor). In the case of solar wind compression, the location of Ganymede's footprint shifts toward the pole, during times of quiet volcanic activity on Io. On the other hand, Ganymede's footprint shifts slightly equatorward when the density of the Io plasma torus sufficiently increases. Moreover, we find a specific case where the Ganymede footprint was detected after a

strong volcanic eruption and solar wind forward shock. This case shows similar locations of Ganymede's footprint while considering different DOYs, possibly as a result of the balancing between internal and external factors. For the internal factor, Iogenic mass outflow from Io affects the radial stretching of Jupiter's magnetic field. On the contrary, for the external factor, the solar wind compression causes the size of Jupiter's magnetosphere to decrease which could affect the poleward shift of mapped magnetic field lines.

For four cases indicated in Figures 4 and 6, the footprint was observed to be shifted either poleward or equatorward when Ganymede was expected to locate at similar locations. The detected shifts of Ganymede's footprint locations appear to be under the influences from inside and outside the magnetosphere, that is, internal and external factors, that modify the magnetic field mapping from Ganymede location to the footprint emission in the ionosphere. For the comparison between the internal and external factors, we consider the variation of plasma density in Jupiter's magnetosphere which is related to the volcanic eruption on Io as the internal factor and the solar wind compression as the external factor. For Case 1, Ganymede's footprint detected on DOY 054 shifted in the poleward direction in comparison to Ganymede's footprint detected on DOY 068. There were continuous volcanic eruptions on Io during February and March 2007 (Spencer et al., 2007). Therefore, the mass loading rate (\dot{M}) increased due to the additional volcanic materials from Io, resulting in an increase in cold plasma density in the magnetosphere, which affects the magnetic field line stretching and Ganymede's footprint locations detected on both DOY 054 and DOY 068. Moreover, the polar projections (Figures 6a and 6b) show dawn brightening on DOY 054, associating to the result of the solar wind propagation model which is presented by Clarke et al. (2009) using magnetohydrodynamic (MHD) model by Zieger and Hansen (2008). The model shows that the dynamic pressure of solar wind increased during DOY 054, which is approximately 10 times higher than that on DOY 068. Thus, in this case, the results of dawn brightening, and the poleward shifts of the main emission as shown in Figure 6a could correspond to the solar wind forward shock causing the smaller size of the magnetosphere. Therefore, the poleward shift on DOY 054 could be related to the external factor consistent with the result from the magnetodisc model (dashed lines in Figure 5b).

For Case 2, Ganymede's footprint was at similar locations on DOY 132, DOY 154, and DOY 161 as shown by the polar projection in Figures 6c–6e. For the internal factor, Jupiter's aurora on DOY 154 was detected after a strong volcanic eruption on Io which took place at the end of May (approximately on DOY 151) (Bonfond et al., 2012). In addition, Yoneda et al. (2009) presented the enhancement of sodium nebular including the brightening of Io plasma torus on the dusk side which took place from DOY 139 to DOY 154 and then decreased after DOY 159. While the polar projections (Figures 6c–6e) show the similar emission on DOY 132 and DOY 161, but, on DOY 154, outer emission in the equatorward direction from the main emission was detected. Moreover, Ganymede's footprint on DOY 154 was detected after the solar wind forward shock (Clarke et al., 2009). The magnetospheric plasma density was increased due to volcanic materials from Io in combination with the decrease of the angular velocity of the plasma disk causing the magnetic field line to stretch, accordingly causing the equatorward shift of Ganymede's footprint. On the contrary, the solar wind causes the compression of the magnetosphere which is associated with a decrease in magnetopause distance. As a result, the curvature of the field lines decreases and causes the poleward shifts of Ganymede's footprint. Thus, this event could be affected by the internal factor from the enhancement of cold plasma density being transported outward, and at the same time by the external factor from solar wind compression, which would generate the hot plasma heating associated with the increase of K_h . Specifically, for DOY 154 data, both factors seem to affect the magnetic field mapping in opposite direction. Consequently, Ganymede's footprint location did not shift significantly and was detected to be at similar locations on DOY 132 and DOY 161. This case is consistent with the result from the magnetodisc model for the balance between increasing K_h (blue solid line) and compressed magnetosphere (yellow dashed line), as shown in Figure 5a. The enhancement of K_h could be associated with the magnetosphere shrinkage due to the adiabatic compression while the solar wind compression reduces the magnetopause size from 80 to 50 R_J .

For Case 3, Ganymede's footprint detected on DOY 199 shifted poleward from Ganymede's footprint detected on DOY 178. Based on Io plasma torus emission observations by Extreme Ultraviolet Spectroscope for Exospheric Dynamics onboard the Hisaki satellite (Tsuchiya et al., 2019), there was no evidence of strong volcanic eruptions on Io during the HST observations of these two events. The polar projection (Figure 6g) shows that Jupiter's main emission shifted poleward between system III longitude $\sim 150^\circ$ – 180° on DOY 199 in comparison with those observed on DOY 178 (Figure 6f). The poleward shift of the main emission could correspond to the decreases of magnetic field curvature due to solar wind compression. As a result, the size of the magnetosphere decreases, and the magnetic field lines are mapped to higher latitudes. Additionally, the contraction of Jupiter's magnetosphere

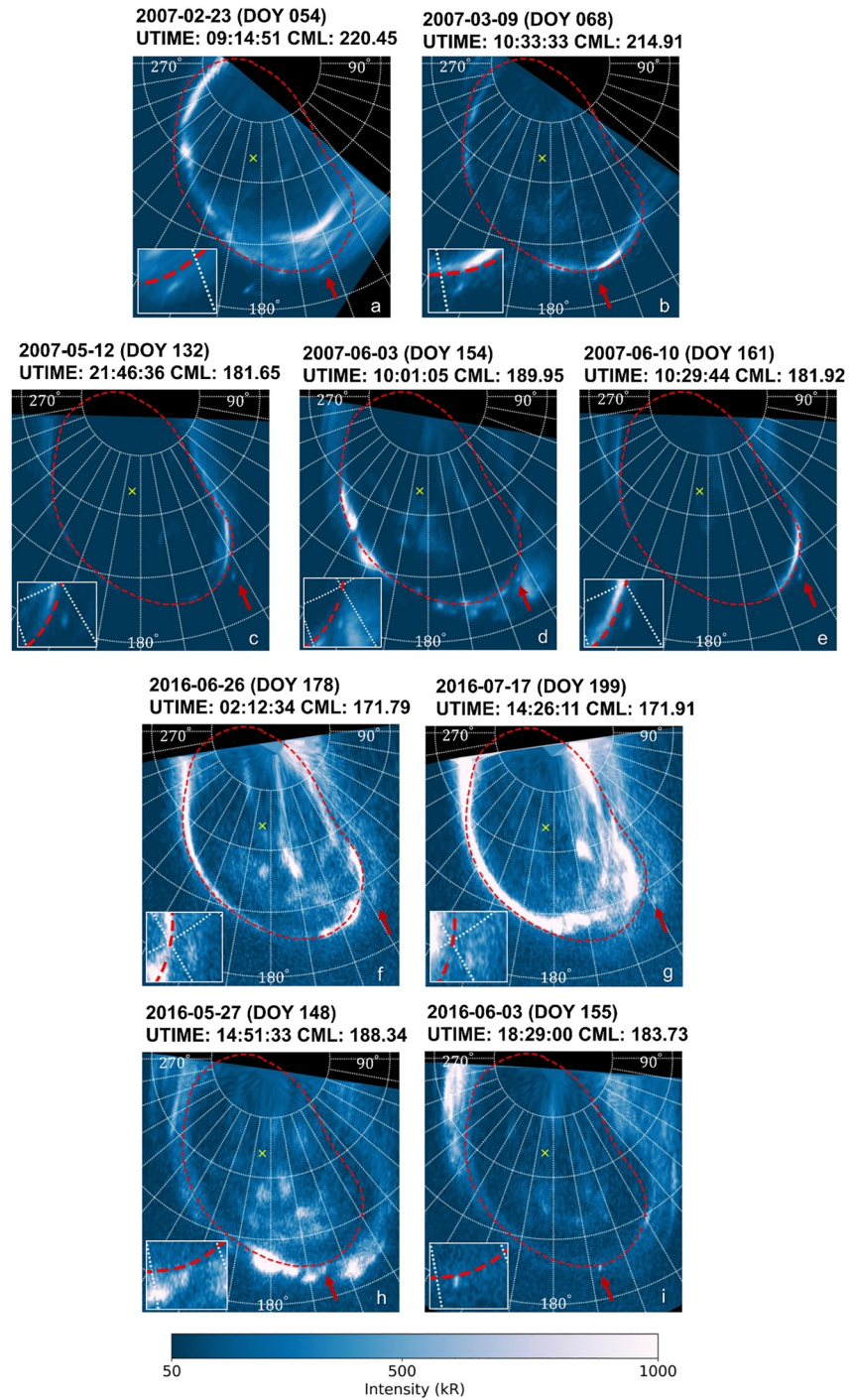


Figure 6. Polar projections for four cases as labeled in Figure 4, where a and b are for Case 1, c–e for Case 2, f and g for Case 3, and h and i for Case 4. The average position of the main emission is presented as a red dashed line. The red arrows indicate the positions of Ganymede's footprint.

due to the solar wind compression could affect the slightly poleward shift of Ganymede's locations on DOY 199 in comparison to Ganymede's footprint locations on DOY 178. This case is similar to Case 1, where the location of Ganymede's footprint is affected by the external factor. The compression could cause the increase of K_p in Jupiter's magnetosphere compatible with the dashed lines in Figure 5a. Although, there is a correlation between the shrinking of the main emission and the poleward shift of the footprint, the mapped location of the main emission

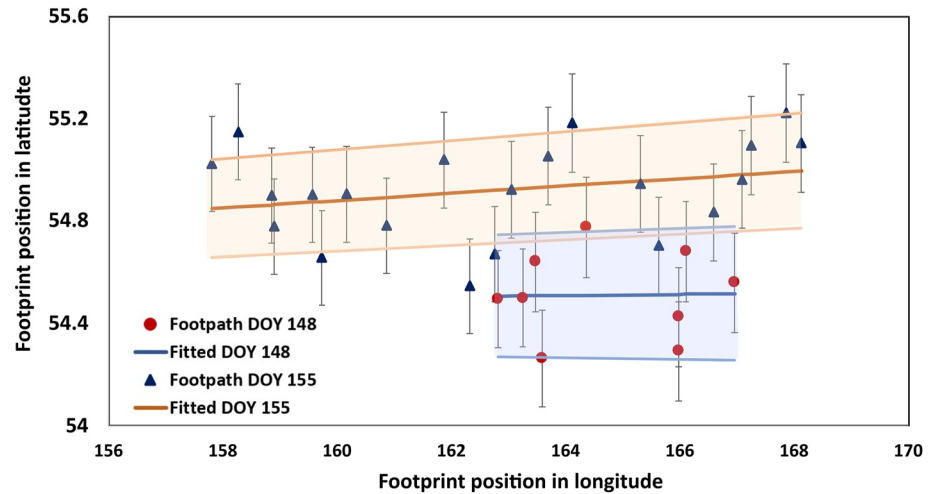


Figure 7. The footpath of Ganymede's footprint and the uncertainty within a standard deviation for Case 4 as shown in Figures 6h and 6i, between DOY 148 (red circles) and DOY 155 (blue triangles). Blue and orange shaded areas indicate the uncertainty of Ganymede's footpaths on DOY 148 and DOY 155, respectively.

from Jupiter's magnetosphere is very complicated. The effects of the magnetospheric compression could cause both the stretching of the magnetic field and the location of the source of the main emission in the magnetosphere, while the source of Ganymede magnetic footprint is always located at $\sim 15 R_J$.

For Case 4, Ganymede's footprint detected on DOY 148 shifted equatorward from Ganymede's footprint detected on DOY 155. Both events were detected during the decrease of the rotation of Io plasma torus on System IV period (Tsuchiya et al., 2019). This result is consistent with Nichols (2011) who showed the increased mass loading from volcanic materials from Io associated with the increase of plasma density causes the angular momentum to decrease. In addition, Tsuchiya et al. (2019) presented the increases in the azimuthal amplitudes of torus composition (SIV/SII) variations associated with the increases in thermal electron temperature from the middle of May to June 2016. The amplitude of torus composition ratio (SIV/SII) variations on DOY 148 appeared to be higher than that on DOY 155. However, both Ganymede's footprint positions on DOY 148 and DOY 155 were detected during the decreases in the angular velocity of the Io plasma torus as mentioned above. Thus, for Case 4, we plotted the Ganymede footpaths and uncertainty within a standard deviation as shown in Figure 7. On average, the data in DOY 155 are at higher latitudes than the data in DOY 148, where the difference is in the border of the measurement uncertainty. The high variation of Ganymede's footprint positions on both days is because the footprint was coincident with the main emission, as shown in Figures 6h and 6i. Accordingly, Ganymede's footprint was sometimes very dim, and thus the positions appear to wriggle. In addition, Kita et al. (2019) presented similar values of solar wind dynamic pressure observed on DOY 148 and DOY 155. The polar projections in Figures 6h and 6i show the equatorward shift of Ganymede's footprint location on DOY 148 in comparison to the footprint on DOY 155. Thus, Ganymede's footprint locations in Case 4 could be mainly affected by the internal factors, from which the increase of plasma density caused the equatorward shift of Ganymede's footprint location on DOY 148, as shown in Figure 5b.

6. Summary

The modeled magnetic field mapping is employed in this work to indicate the connection between Ganymede's footprint location and the variation of magnetospheric plasma as well as the external factor, which is mainly from the solar wind compression. The location shifts of Ganymede's footprint in 2007 and 2016 appear to have possible connections with the increase of plasma density, relating to the mass loading from volcanic materials from Io as well as the compression from the solar wind. The location shifts are considered separately in four cases.

- Case 1 (DOY 054 and DOY 068) and Case 3 (DOY 178 and DOY 199): Ganymede's footprint locations slightly shifted poleward. This shift could be consistent with the result from the magnetodisc model while considering the effect of solar wind compression. Under the solar wind compression, where the size of the

magnetosphere decreases, the mapped magnetic footprint shifts in a poleward direction, as shown in Figure 5 (dashed line).

- Case 2 (DOY 132, DOY 154, and DOY 161): The increases of K_h affects the limit of azimuthal current on the equatorial plane, resulting in the stretching of the magnetic field lines as shown in Figure 5a, which causes the equatorward shift of Ganymede's footprint. In Figure 5a, for $K_h = 1.25 \times 10^7 \text{ Pa m T}^{-1}$, the field line is mapped poleward with the consideration of the solar wind compression (red dashed line). For the case of, $K_h = 3.5 \times 10^7 \text{ Pa m T}^{-1}$, the compression resulting in the poleward shift (yellow dashed line) and the magnetic field lines are mapped to similar locations for the case of no compression $K_h = 2.5 \times 10^7 \text{ Pa m T}^{-1}$ (blue solid line). Consequently, there is compensation between an increase of K_h and the solar wind compression, as shown in Figure 4b.
- Case 4 (DOY 148 and DOY 155): During May–July 2016, Tsuchiya et al. (2019) showed that the slower rotation period of Io plasma torus on system IV could be caused by the increased mass loading originating from Io's volcanic materials, consistent with the result from Nichols (2011). Thus, the equatorward shifts of Ganymede's footprint locations could be influenced by the mass loading rate (\dot{M}) enhancement from volcanic activity on Io which eventually results in the enhancement of the plasma sheet density in Jupiter's magnetosphere as shown in Figure 5b, agreeing with the magnetic field line mapping by magnetodisc model (Nichols et al., 2015).

Overall, the results in this work emphasize the effects of the internal and external factors on the location of Ganymede's footprint. However, the effects of solar wind compression on the azimuthal current density will be studied further in more detail in terms of the comparison of several auroral features including their intensities.

Data Availability Statement

Jupiter's aurora images in this work are available at https://archive.stsci.edu/proposal_search.php?mission=hst&id=10862 for 2007 data and https://archive.stsci.edu/proposal_search.php?mission=hst&id=14105 for 2016 data. The predicted Ganymede footprint location in the northern hemisphere using the JRM33 model from Supporting Information by Connerney et al. (2022) <https://doi.org/10.1029/2021JE007055>.

References

- Adriani, A., Filacchione, G., Di Iorio, T., Turrini, D., Noschese, R., Cicchetti, A., et al. (2017). JIRAM, the Jovian infrared auroral mapper. *Space Science Reviews*, 213(1–4), 393–446. <https://doi.org/10.1007/s11214-014-0094-y>
- Bagenal, F., & Delamere, P. A. (2011). Flow of mass and energy in the magnetospheres of Jupiter and Saturn. *Journal of Geophysical Research*, 116(A5), A05209. <https://doi.org/10.1029/2010JA016294>
- Bagenal, F., Dougherty, L. P., Bodisch, K. M., Richardson, J. D., & Belcher, J. M. (2017). Survey of Voyager plasma science ions at Jupiter: 1. Analysis method. *Journal of Geophysical Research: Space Physics*, 122(8), 8241–8256. <https://doi.org/10.1002/2016JA023797>
- Bodisch, K. M., Dougherty, L. P., & Bagenal, F. (2017). Survey of Voyager plasma science ions at Jupiter: 3. Protons and minor ions. *Journal of Geophysical Research: Space Physics*, 122(8), 8277–8294. <https://doi.org/10.1002/2017JA024148>
- Bolton, S. J., Thorne, R. M., Gurnett, D. A., Kurth, W. S., & Williams, D. J. (1997). Enhanced whistler-mode emissions: Signatures of interchange motion in the Io torus. *Geophysical Research Letters*, 24(17), 2123–2126. <https://doi.org/10.1029/97GL02020>
- Bonfond, B. (2010). The 3-D extent of the Io UV footprint on Jupiter. *Journal of Geophysical Research*, 115(A9). <https://doi.org/10.1029/2010JA015475>
- Bonfond, B., Grodent, D., Gérard, J. C., Radioti, A., Saur, J., & Jacobsen, S. (2008). UV Io footprint leading spot: A key feature for understanding the UV Io footprint multiplicity? *Geophysical Research Letters*, 35(5), L05107. <https://doi.org/10.1029/2007GL032418>
- Bonfond, B., Grodent, D., Gérard, J. C., Stallard, T., Clarke, J. T., Yoneda, M., et al. (2012). Auroral evidence of Io's control over the magnetosphere of Jupiter. *Geophysical Research Letters*, 39(1), L01105. <https://doi.org/10.1029/2011GL050253>
- Bonfond, B., Hess, S., Bagenal, F., Gérard, J.-C., Grodent, D., Radioti, A., et al. (2013a). The multiple spots of the Ganymede auroral footprint. *Geophysical Research Letters*, 40(19), 4977–4981. <https://doi.org/10.1002/grl.50989>
- Bonfond, B., Hess, S., Gérard, J. C., Grodent, D., Radioti, A., Chantry, V., et al. (2013). Evolution of the Io footprint brightness I: Far-UV observations. *Planetary and Space Science*, 88, 64–75. <https://doi.org/10.1016/j.pss.2013.05.023>
- Bonfond, B., Saur, J., Grodent, D., Badman, S. V., Bisikalo, D., Schematovich, V., et al. (2017). The tails of the satellite auroral footprints at Jupiter. *Journal of Geophysical Research: Space Physics*, 122(8), 7985–7996. <https://doi.org/10.1002/2017JA024370>
- Caudal, G. (1986). A self-consistent model of Jupiter's magnetodisc including the effects of centrifugal force and pressure. *Journal of Geophysical Research*, 91(A4), 4201–4221. <https://doi.org/10.1029/JA091iA04p04201>
- Clarke, J. T., Ajello, J., Ballester, G., Ben Jaffel, L., Connerney, J., Gérard, J. C., et al. (2002). Ultraviolet emissions from the magnetic footprints of Io, Ganymede and Europa on Jupiter. *Nature*, 415(6875), 997–1000. <https://doi.org/10.1038/415997a>
- Clarke, J. T., Grodent, D., Cowley, S. W. H., Bunce, E. J., Zarka, P., Connerney, J. E. P., & Satoh, T. (2004). Jupiter's aurora. In F. Bagenal, T. E. Dowling, & W. B. McKinnon (Eds.), *Jupiter: the planet, satellites and magnetosphere* (pp. 639–670).
- Clarke, J. T., Nichols, J., Gérard, J. C., Grodent, D., Hansen, K. C., Kurth, W., et al. (2009). Response of Jupiter's and Saturn's auroral activity to the solar wind. *Journal of Geophysical Research*, 114(A5), A05210. <https://doi.org/10.1029/2008JA013694>

Acknowledgments

The work is based on observation by NASA/ESA Hubble Space Telescope, obtained at the Space Telescope Science Institute, which is operated by AURA Inc., for NASA. The aurora images were achieved by J. T. Clarke which was supported by Grant HST-GO-10862.01-A from STScI to Boston University (https://archive.stsci.edu/proposal_search.php?mission=hst&id=10862). J. D. Nichols from Leicester University (program GO 14105). The data are available at STScI (https://archive.stsci.edu/proposal_search.php?mission=hst&id=14105). This research was partly supported by the National Astronomical Research Institute of Thailand (NARIT) and Thailand Science Research and Innovation (TSRI) Grant RTA6280002.

- Connerney, J. E. P., Acuna, M. H., & Ness, N. F. (1981). Modeling the Jovian current sheet and inner magnetosphere. *Journal of Geophysical Research*, *86*(A10), 8370–8384. <https://doi.org/10.1029/JA086iA10p08370>
- Connerney, J. E. P., Kotsiaros, S., Oliverson, R. J., Espley, J. R., Joergensen, J. L., Joergensen, P. S., et al. (2018). A New model of Jupiter's magnetic field from Juno's first nine orbits. *Geophysical Research Letters*, *45*(6), 2590–2596. <https://doi.org/10.1002/2018GL077312>
- Connerney, J. E. P., Timmins, S., Hecceg, M., & Joergensen, J. L. (2020). A Jovian magnetodisc model for the Juno era. *Journal of Geophysical Research: Space Physics*, *125*(10), e28138. <https://doi.org/10.1029/2020JA028138>
- Connerney, J. E. P., Timmins, S., Oliverson, R. J., Espley, J. R., Joergensen, J. L., Kotsiaros, S., et al. (2022). A new model of Jupiter's magnetic field at the completion of Juno's prime mission. *Journal of Geophysical Research: Planets*, *127*(2), e07055. <https://doi.org/10.1029/2021JE007055>
- Cowley, S. W. H., & Bunce, E. J. (2001). Origin of the main auroral oval in Jupiter's coupled magnetosphere-ionosphere system. *Planetary and Space Science*, *49*(10–11), 1067–1088. [https://doi.org/10.1016/S0032-0633\(00\)00167-7](https://doi.org/10.1016/S0032-0633(00)00167-7)
- Dougherty, L. P., Bodisch, K. M., & Bagenal, F. (2017). Survey of Voyager plasma science ions at Jupiter: 2. Heavy ions. *Journal of Geophysical Research: Space Physics*, *122*(8), 8257–8276. <https://doi.org/10.1002/2017JA024053>
- Drell, S. D., Foley, H. M., & Ruderman, M. A. (1965). Drag and propulsion of large satellites in the ionosphere: An Alfvén propulsion engine in space. *Journal of Geophysical Research*, *70*(13), 3131–3145. <https://doi.org/10.1029/JZ070i013p03131>
- Frank, L. A., & Paterson, W. R. (2002). Galileo observations of electron beams and thermal ions in Jupiter's magnetosphere and their relationship to the auroras. *Journal of Geophysical Research*, *107*(A12), 1478–SMP35-17. <https://doi.org/10.1029/2001JA009150>
- Gershman, D. J., Connerney, J. E. P., Kotsiaros, S., DiBraccio, G. A., Martos, Y. M., Viñas, A. F., et al. (2019). Alfvénic fluctuations associated with Jupiter's auroral emissions. *Geophysical Research Letters*, *46*(13), 7157–7165. <https://doi.org/10.1029/2019GL082951>
- Grodent, D., Bonfond, B., Radioti, A., Gérard, J.-C., Jia, X., Nichols, J. D., & Clarke, J. T. (2009). Auroral footprint of Ganymede. *Journal of Geophysical Research*, *114*(A7), A07212. <https://doi.org/10.1029/2009JA014289>
- Grodent, D., Gérard, J.-C., Radioti, A., Bonfond, B., & Saglam, A. (2008). Jupiter's changing auroral location. *Journal of Geophysical Research*, *113*(A1), A01206. <https://doi.org/10.1029/2007JA012601>
- Gustin, J., Bonfond, B., Grodent, D., & Gérard, J. C. (2012). Conversion from HST ACS and STIS auroral counts into brightness, precipitated power, and radiated power for H2 giant planets. *Journal of Geophysical Research*, *117*(A7), A07316. <https://doi.org/10.1029/2012JA017607>
- Hess, S. L. G., Delamere, P., Dols, V., Bonfond, B., & Swift, D. (2010). Power transmission and particle acceleration along the Io flux tube. *Journal of Geophysical Research*, *115*(A6), A06205. <https://doi.org/10.1029/2009JA014928>
- Hill, T. W. (1979). Inertial limit on corotation. *Journal of Geophysical Research*, *84*(A11), 6554–6558. <https://doi.org/10.1029/JA084iA11p06554>
- Jia, X., Walker, R. J., Kivelson, M. G., Khurana, K. K., & Linker, J. A. (2008). Three-dimensional MHD simulations of Ganymede's magnetosphere. *Journal of Geophysical Research*, *113*(A6), A06212. <https://doi.org/10.1029/2007JA012748>
- Khurana, K. K., Kivelson, M. G., Vasylunas, V. M., Krupp, N., Woch, J., Lagg, A., et al. (2004). The configuration of Jupiter's magnetosphere. In F. Bagenal, T. E. Dowling, & W. B. McKinnon (Eds.), *Jupiter: the planet, satellites and magnetosphere* (Vol. 1, pp. 593–616).
- Khurana, K. K., & Schwarzl, H. K. (2005). Global structure of Jupiter's magnetospheric current sheet. *Journal of Geophysical Research*, *110*(A7), A07227. <https://doi.org/10.1029/2004JA010757>
- Kita, H., Kimura, T., Tao, C., Tsuchiya, F., Murakami, G., Yamazaki, A., et al. (2019). Jovian UV aurora's response to the solar wind: Hisaki EXCEED and Juno observations. *Journal of Geophysical Research: Space Physics*, *124*(12), 10209–10218. <https://doi.org/10.1029/2019JA026997>
- Kivelson, M. G., Bagenal, F., Kurth, W. S., Neubauer, F. M., Paranicas, C., & Saur, J. (2004). *Magnetospheric interactions with satellites*. In F. Bagenal, T. E. Dowling, & W. B. McKinnon (Eds.), (pp. 513–536).
- Kivelson, M. G., Khurana, K. K., Coroniti, F. V., Joy, S., Russell, C. T., Walker, R. J., et al. (1997). The magnetic field and magnetosphere of Ganymede. *Geophysical Research Letters*, *24*(17), 2155–2158. <https://doi.org/10.1029/97GL02201>
- Krimigis, S. M., Carbary, J. F., Keath, E. P., Bostrom, C. O., Axford, W. I., Gloeckler, G., et al. (1981). Characteristic of hot plasma in the Jovian magnetosphere: Results from the Voyager spacecraft. *Journal of Geophysical Research*, *86*(A10), 8227–8257. <https://doi.org/10.1029/JA086iA10p08227>
- Krupp, N., Vasylunas, V. M., Woch, J., Lagg, A., Khurana, K. K., Kivelson, M. G., et al. (2004). Dynamics of the Jovian magnetosphere. In F. Bagenal, T. E. Dowling, & W. B. McKinnon (Eds.) *Jupiter: the planet, satellites and magnetosphere* (Vol. 1, pp. 617–638).
- Lysak, R. L., & Song, Y. (2003). Kinetic theory of the Alfvén wave acceleration of auroral electrons. *Journal of Geophysical Research*, *108*(A4), 8005. <https://doi.org/10.1029/2002JA009406>
- McComas, D. J., Alexander, N., Allegrini, F., Bagenal, F., Beebe, C., Clark, G., et al. (2017). The Jovian auroral distributions experiment (JADE) on the Juno mission to Jupiter. *Space Science Reviews*, *213*(1–4), 547–643. <https://doi.org/10.1007/s11214-013-9990-9>
- McComas, D. J., Szalay, J. R., Allegrini, F., Bagenal, F., Connerney, J., Ebert, R. W., et al. (2017). Plasma environment at the dawn flank of Jupiter's magnetosphere: Juno arrives at Jupiter. *Geophysical Research Letters*, *44*(10), 4432–4438. <https://doi.org/10.1002/2017GL072831>
- McNutt, R. L., Belcher, J. W., & Bridge, H. S. (1981). Positive ion observations in the middle magnetosphere of Jupiter. *Journal of Geophysical Research*, *86*(A10), 8319–8342. <https://doi.org/10.1029/JA086iA10p08319>
- Moirano, A., Gomez Casajus, L., Zannoni, M., Durante, D., & Tortora, P. (2021). Morphology of the IO plasma torus from Juno radio occultations. *Journal of Geophysical Research*, *126*(10), e29190. <https://doi.org/10.1029/2021JA029190>
- Moirano, A., Mura, A., Adriani, A., Dols, V., Bonfond, B., Waite, J. H., et al. (2021). Morphology of the auroral tail of Io, Europa, and Ganymede from JIRAML-band imager. *Journal of Geophysical Research: Space Physics*, *126*(9), e2021JA029450. <https://doi.org/10.1029/2021JA029450>
- Mura, A., Adriani, A., Connerney, J. E. P., Bolton, S., Altieri, F., Bagenal, F., et al. (2018). Juno observations of spot structures and a split tail in Io-induced aurorae on Jupiter. *Science*, *361*(6404), 774–777. <https://doi.org/10.1126/science.aat1450>
- Nichols, J. D. (2011). Magnetosphere-ionosphere coupling in Jupiter's middle magnetosphere: Computations including a self-consistent current sheet magnetic field model. *Journal of Geophysical Research*, *116*(A10), A10232. <https://doi.org/10.1029/2011JA016922>
- Nichols, J. D., Achilleos, N., & Cowley, S. W. H. (2015). A model of force balance in Jupiter's magnetodisc including hot plasma pressure anisotropy. *Journal of Geophysical Research: Space Physics*, *120*(12), 10185–10206. <https://doi.org/10.1002/2015JA021807>
- Nichols, J. D., Allegrini, F., Bagenal, F., Bunce, E. J., Cowley, S. W. H., Ebert, R. W., et al. (2020). An enhancement of Jupiter's main auroral emission and magnetospheric currents. *Journal of Geophysical Research: Space Physics*, *125*(8), e27904. <https://doi.org/10.1029/2020JA027904>
- Nichols, J. D., Badman, S. V., Bagenal, F., Bolton, S. J., Bonfond, B., Bunce, E. J., et al. (2017). Response of Jupiter's auroras to conditions in the interplanetary medium as measured by the Hubble Space Telescope and Juno. *Geophysical Research Letters*, *44*(15), 7643–7652. <https://doi.org/10.1002/2017GL073029>
- Nichols, J. D., Clarke, J. T., Gérard, J. C., Grodent, D., & Hansen, K. C. (2009). Variation of different components of Jupiter's auroral emission. *Journal of Geophysical Research*, *114*(A6), A06210. <https://doi.org/10.1029/2009JA014051>
- Paty, C., Paterson, W., & Winglee, R. (2008). Ion energization in Ganymede's magnetosphere: Using multifluid simulations to interpret ion energy spectrograms. *Journal of Geophysical Research*, *113*(A6), A06211. <https://doi.org/10.1029/2007JA012848>

- Plainaki, C., Lilensten, J., Radioti, A., Andriopoulou, M., Milillo, A., Nordheim, T. A., et al. (2016). Planetary space weather: Scientific aspects and future perspectives. *Journal of Space Weather and Space Climate*, 6, A31. <https://doi.org/10.1051/swsc/2016024>
- Plainaki, C., Milillo, A., Massetti, S., Mura, A., Jia, X., Orsini, S., et al. (2015). The H₂O and O₂ exospheres of Ganymede: The result of a complex interaction between the Jovian magnetospheric ions and the icy moon. *Icarus*, 245, 306–319. <https://doi.org/10.1016/j.icarus.2014.09.018>
- Pontius, D. H. (1997). Radial mass transport and rotational dynamics. *Journal of Geophysical Research*, 102(A4), 7137–7150. <https://doi.org/10.1029/97JA00289>
- Roth, L., Boissier, J., Moullet, A., Sánchez-Monge, Á., de Kleer, K., Yoneda, M., et al. (2020). An attempt to detect transient changes in Io's SO₂ and NaCl atmosphere. *Icarus*, 350, 113925. <https://doi.org/10.1016/j.icarus.2020.113925>
- Saur, J., Grambusch, T., Duling, S., Neubauer, F. M., & Simon, S. (2013). Magnetic energy fluxes in sub-Alfvénic planet star and moon planet interactions. *A&A*, 552, A119. <https://doi.org/10.1051/0004-6361/201118179>
- Saur, J., Neubauer, F. M., Strobel, D. F., & Summers, M. E. (1999). Three-dimensional plasma simulation of Io's interaction with the Io plasma torus: Asymmetric plasma flow. *Journal of Geophysical Research*, 104(A11), 25105–25126. <https://doi.org/10.1029/1999JA900304>
- Schlegel, S., & Saur, J. (2022). Alternating emission features in Io's footprint tail: Magnetohydrodynamical simulations of possible causes. *Journal of Geophysical Research: Space Physics*, 127(5), e30243. <https://doi.org/10.1029/2021JA030243>
- Spencer, J. R., Stern, S. A., Cheng, A. F., Weaver, H. A., Reuter, D. C., Retherford, K., et al. (2007). Io volcanism seen by new horizons: A major eruption of the Tvashtar volcano. *Science*, 318(5848), 240–243. <https://doi.org/10.1126/science.1147621>
- Steffl, A. J., Delamere, P. A., & Bagenal, F. (2008). Cassini UVIS observations of the Io plasma torus. IV. Modeling Temporal and Azimuthal Variability, 194(1), 153–165. <https://doi.org/10.1016/j.icarus.2007.09.019>
- Sulaiman, A. H., Hospodarsky, G. B., Elliott, S. S., Kurth, W. S., Gurnett, D. A., Imai, M., et al. (2020). Wave-particle interactions associated with Io's auroral footprint: Evidence of Alfvén, ion cyclotron, and whistler modes. *Geophysical Research Letters*, 47(22), e88432. <https://doi.org/10.1029/2020GL088432>
- Szalay, J. R., Allegrini, F., Bagenal, F., Bolton, S. J., Bonfond, B., Clark, G., et al. (2020). Alfvénic acceleration sustains Ganymede's footprint tail aurora. *Geophysical Research Letters*, 47(3), e86527. <https://doi.org/10.1029/2019GL086527>
- Tao, C., Badman, S. V., & Fujimoto, M. (2011). UV and IR auroral emission model for the outer planets: Jupiter and Saturn comparison. *Icarus*, 213(2), 581–592. <https://doi.org/10.1016/j.icarus.2011.04.001>
- Tsuchiya, F., Arakawa, R., Misawa, H., Kagitani, M., Koga, R., Suzuki, F., et al. (2019). Azimuthal variation in the IO plasma torus observed by the Hisaki satellite from 2013 to 2016. *Journal of Geophysical Research: Space Physics*, 124(5), 3236–3254. <https://doi.org/10.1029/2018JA026038>
- Tsuchiya, F., Yoshioka, K., Kimura, T., Koga, R., Murakami, G., Yamazaki, A., et al. (2018). Enhancement of the Jovian magnetospheric plasma circulation caused by the change in plasma supply from the satellite Io. *Journal of Geophysical Research: Space Physics*, 123(8), 6514–6532. <https://doi.org/10.1029/2018JA025316>
- Vogt, M. F., Bunce, E. J., Kivelson, M. G., Khurana, K. K., Walker, R. J., Radioti, A., et al. (2015). Magnetosphere-ionosphere mapping at Jupiter: Quantifying the effects of using different internal field models. *Journal of Geophysical Research: Space Physics*, 120(4), 2584–2599. <https://doi.org/10.1002/2014JA020729>
- Wannawichian, S., Clarke, J. T., & Nichols, J. D. (2010). Ten years of Hubble Space Telescope observations of the variation of the Jovian satellites' auroral footprint brightness. *Journal of Geophysical Research*, 115(A2), A02206. <https://doi.org/10.1029/2009JA014456>
- Yoneda, M., Kagitani, M., & Okano, S. (2009). Short-term variability of Jupiter's extended sodium nebula. *Icarus*, 204(2), 589–596. <https://doi.org/10.1016/j.icarus.2009.07.023>
- Yoneda, M., Kagitani, M., Tsuchiya, F., Sakanoi, T., & Okano, S. (2015). Brightening event seen in observations of Jupiter's extended sodium nebula. *Icarus*, 261, 31–33. <https://doi.org/10.1016/j.icarus.2015.07.037>
- Yoneda, M., Tsuchiya, F., Misawa, H., Bonfond, B., Tao, C., Kagitani, M., & Okano, S. (2013). Io's volcanism controls Jupiter's radio emissions. *Geophysical Research Letters*, 40(4), 671–675. <https://doi.org/10.1002/grl.50095>
- Zieger, B., & Hansen, K. C. (2008). Statistical validation of a solar wind propagation model from 1 to 10 AU. *Journal of Geophysical Research*, 113(A8), A08107. <https://doi.org/10.1029/2008JA013046>